2D Numerical Simulation Study of Airfoil Performance

Nasser Shelil and Fahad Awjah Almehmadi

Department of Applied Mechanical Engineering, College of Applied Engineering, Muzahimiyah Branch, King Saud University, P.O. Box 800, Riyadh 11421, Saudi Arabia

5   *Correspondence to*: Nasser Shelil (nshelil@ksu.edu.sa)

Abstract. The aerodynamic characteristics of DTU-LN221 airfoil is studied. ANSYS Fluent is used to simulate the airfoil performance with six different turbulence models. The simulation results for the airfoil with different turbulence models are compared with the wind tunnel experimental data performed under the same operating conditions. Results show that there is a beneficial coalition between the predicted values of aerodynamic force coefficients; that are obtained by using computational

10   fluid dynamics simulation, with the wind tunnel experimental data; especially with the angle of attack between -5º to 10º. The Reynolds stress model is chosen to investigate the flow field structure and the surface pressure coefficients under different angles of attack between -5º to 10º. Also the effect of changing air temperature, velocity and turbulence intensity on lift and drag coefficients/forces are examined. The results show that it is recommended to operate the wind turbines airfoil at low air temperature and high velocity to enhance the performance of the wind turbines.

15   **Keywords.** Airfoil – Wind Turbine – CFD – Turbulence Models – Simulation – Aerodynamic Performance – Lift and Drag.

1 Introduction

The trend of using renewable energy resources has increased significantly during the past decade. The usage of wind power is a promising technology for this generation that can help the world to eliminate the dependency on fossil fuel based energy sources such as oil and gas. It also helps the environment to flourish without greenhouse effects or other pollutants. The wind

20   turbine technology offers electrical energy with lower installation and maintenance costs compared to the other energy sources. It is clean, eco-friendly and promotes national security at a time when the decreasing global reserves of fossil fuels is an eminent danger in the sustainability of global economy (Karthikeyan et al., 2015).

The airfoil is a basic element of a wind turbine blade, and its aerodynamic characteristics have a major influence on the wind energy conversion efficiency. The airfoil is the cross section of a wind turbine blade that is used to generate mechanical force

25   due to the motion of air around the airfoil. The design of wind turbine airfoils is a basic but important task for designing optimal wind turbine rotors. Different types of airfoils are used along the blades in order to generate energy from the wind. Both the pressure differences between upper and lower sides of the airfoil together with the friction forces result in an aerodynamic force. This is then divided into the components parallel (drag) and perpendicular (lift) to the oncoming flow. The lift and drag coefficients are obtained by normalizing these forces with the dynamic pressure and the reference area. Both lift

30   and drag coefficients are used to characterize and compare airfoils.

Lift and drag forces on an airfoil are influenced by the angle of attack (AOA), which is the angle between the distributed wind direction and the chord of the airfoil (John D. Anderson, 2017). In order to enhance the performance from the rotor, it is necessary to maximize the lift force and minimize the drag force by optimizing the AOA to obtain the best performance. For the rotor, it would be better to maximize the in-plane component to maximize the torque. This is neither the lift nor the drag

35   directions. Maximizing the power off-take is a desired result thus the turning speed plays an essential role. For improved power, a higher turning speed at lower torque so the turning speed affects the inflow direction is a result of the AOA.

Junwei Yang et al., (Yang et al., 2020) investigated experimentally the effect of turbulent flow on an airfoil with a Gurney flap. The wind tunnel experiments were performed for the DTU-LN221 airfoil under different turbulence levels. The results

demonstrate that under low turbulent inflow conditions, the maximum lift coefficient of the airfoil with flaps increased by 8.47% to 13.50% (i.e., thickness of 0.75%), and the Gurney flap became less effective after stall angle. Other studies are performed to investigate a Gurney flap implementation both experimentally and numerically using Reynolds Average Navier Stoke (RANS) based numerical simulations (Aramendia et al., 2019).

The turbulence model has a significant influence on the numerical simulation results of wind turbine blade airfoil. A traditional numerical simulation process did not consider the impacts of the changed AOA on the simulation results. No matter the amount of the AOA, only one single type of turbulence model was applied to simulate the aerodynamic performance of wind turbine blade airfoil. This simulation method for airfoil aerodynamic performance has a large error result (Wang et al., 2014). The different turbulence models have significant impacts on the aerodynamic performance of a wind turbine blade airfoil. The numerical simulation method for investigating the behavior of flow around the airfoil should have a strong adaptability of low cost, time-saving and ease to reveal the details of the flow field, compared to wind tunnel experiment.

H. Wang et. al., (Wang et al., 2014) compared the aerodynamic simulation results with the theoretical values of the lift coefficients, drag coefficients and the ratio of lift coefficient to drag coefficient. Three different turbulence models were utilized, which are Spallart Allmars (S-A), k-ε RNG, k-ω SST for the prediction of the aerodynamic performance of wind turbine airfoil under different AOA. For the most effective AOA, effects of these three turbulence models on the blade airfoil aerodynamic performance were estimated. For the selected blade airfoil, the simulation results recommended applaying S-A turbulence model before the best AOA and k-ε RNG turbulence model after the best AOA respectively.

Two dimensional airfoil's aerodynamic performance was simulated numerically by Ji Yaoa et al. (Yaoa et al., 2012). The governing equations were Navier-Stokes, and four turbulence models were applied as follows; Standard k-ε model of two equations, RNG k-ε model, Transition SST model of four equations and Reynolds stress model of five equations. The lift coefficient curves of the four turbulence models were much closer to the experimental data, while drag coefficient curves differed largely from the experimental data. This may be caused by the roughness of front edge or other factors. The five equations-Reynolds stress model had the best result amid the four turbulence models.

Aftab et al., (Aftab et al., 2016) studied the Low Reynolds Number flows over airfoil. The turbulence models tested were as follows; one equation S-A, two equation SST k-ω, three equation Intermittency (γ) SST, k-kl-ω and finally, the four equation transition γ-Reθ SST. The results obtained show the values of the experimental study and the current computational fluid dynamics (CFD) study are found to be mutually compatible. This study clearly shows that capturing the transition behaviour, for low Reynolds numbers flows, needs an accurate turbulence model. In the present case, γ-Reθ SST is preferred model as it predicts the flow behavior both at low and high AOA, accurately and in a short duration of time.

Unsteady aerodynamic characteristics was studied by G. H. Yu et.al. (Yu et al., 2010). They used two-dimensional CFD with Menter's transition corrected k−ω SST turbulence model for various reduced frequencies. They observed that flow separation is delayed to higher AOA compared with the static stall case, and the lift force is found to increase far beyond that of the static stall angle. Reduced frequency is observed to have a significant impact on the aerodynamic forces and the pitching moment. The peak in the lift force coefficient appears at a higher AOA with an increasingly reduced frequency.

This work aims to simulate the behavior and performance of an airfoil under different working conditions. A 2D model is considered in Ansys Fluent CFD simulation of the DTU-LN221 airfoil. Six different turbulence models are used to perform the simulations. The simulation results are compared to the experimental data to choose the suitable turbulence model to continue the investigation of the flow characteristics over the airfoil. The effect of the AOA on lift and drag coefficients is investigated. The pressure coefficient is monitored at different angles of attack. The effect of temperature, air velocity and turbulence intensity on the airfoil performance is demonstrated.

2 Methodology

2.1 Experimental Setup

The DTU-LN221 airfoil was designed according to the requirements provided by Lunderskov Møbelfabrik (LM) and tested in the LM wind tunnel (Cheng et al., 2014; 2015a). The design of this type of wind turbine rotors have aerodynamically high efficiency, low cost and low noise emission (Cheng et al., 2014).

The DTU-LN221 airfoil model (Sessarego et al., 2016; Yang et al., 2020; 2015a; Cheng et al., 2014), as shown in Figure 1, has a chord length of 0.6 m and a span of 1.5 m. The airfoil model was vertically placed in the test section. The bottom part of the airfoil section was connected by the rotating shaft, which was fixed on a rotational plate. Therefore, the AOA can be remotely controlled via a shaft connection with a motor below the wind tunnel. The airfoil model was made of aluminum alloy. In the experiment, the free stream flow velocity was 37.5 m/s, and the corresponding Reynolds number based on the airfoil chord length was 1.5×10^6. Although wind turbines often operate at wind speed below 37.5 m/s, in this research the magnitude of the Reynolds number was up to an order of 10^6. Therefore, the experimental value of the Reynolds number was chosen to approach an order of magnitude corresponding to those obtained from full-scale wind turbines (Yang et al., 2020; Roha, 2012). The full description of the design of the airfoil profile is described in details by (Sessarego et al., 2016; Yang et al., 2020). Table 1 shows the basic data for the airfoil and operating conditions of the experimental data (Sessarego et al., 2016; Yang et al., 2020).

Table 1: Basic data chosen for wind-turbine airfoil model

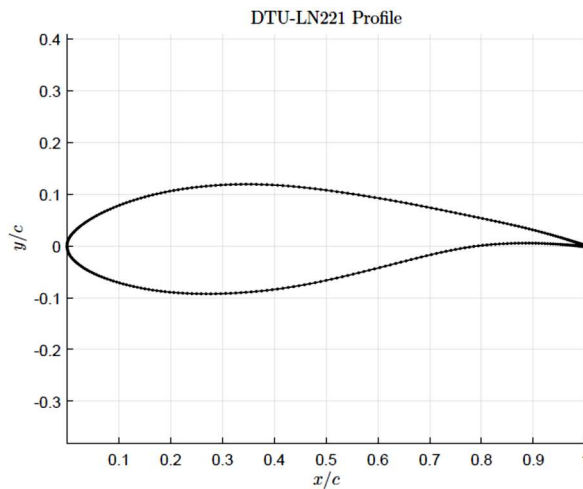| Property	Value
Airfoil name	DTU-LN221
Density of air	1.205 kg/m^3
Dynamic viscosity of air	1.821×10^5 Ns/m^2
Air Temperature	293 K
Design wind speed, Vo	37.5 m/s
Re	1.5×10^6
Airfoil chord	0.600 m
Airfoil thickness relative to chord	21%
Airfoil length	1.5 m
Material	aluminum alloy

Figure 1: Profile coordinates of the DTU-LN221 airfoil (Sessarego et al., 2016)

2.2 Mathematical Modelling

In CFD, Reynolds Average Navier Stoke (RANS) is the most widely used turbulence modelling approach. In this approach, the Navier Stokes equations are split into mean and fluctuating components. The total velocity u_i is a function of the mean velocity $\bar{u}_i$ and the fluctuating velocity $\acute{u}_i$ as shown in the equation below (Hinze, 1975).

$$u_{i\,=}\ \bar{u}_i + \acute{u}_i \tag{1}$$

The continuity and momentum equation incorporating these instantaneous flow variables are given by:

$$\frac{\partial \rho}{\partial t} + \frac{\partial}{\partial x_i}(\rho u_i) = 0 \tag{2}$$

$$\frac{\partial}{\partial t}\rho u_i + \frac{\partial}{\partial x_i}(\rho u_i u_j) = \frac{\partial \rho}{\partial x_i} + \frac{\partial}{\partial x_j}\left[\mu\left(\frac{\partial u_i}{\partial x_j} + \frac{\partial u_j}{\partial x_i} - \frac{2}{3}\delta_{ij}\frac{\partial u_i}{\partial x_i}\right)\right] + \frac{\partial}{\partial x_i}(-\rho \overline{\acute{u}_i \acute{u}_j}) \tag{3}$$

These above equations (in Cartesian tensor form) are known as RANS equations, and the additional Reynolds stress terms $-\rho\overline{\acute{u}_i\acute{u}_j}$ need to be modelled. The Boussinesq hypothesis is applied in relating the Reynolds stress and mean velocity:

$$-\rho\overline{\acute{u}_i\acute{u}_j} = \mu_t\left(\frac{\partial u_i}{\partial x_j} + \frac{\partial u_j}{\partial x_i}\right) - \frac{2}{3}\left(\rho k + \mu_t\frac{\partial u_{ik}}{\partial x_k}\right)\delta_{ij} \tag{4}$$

2.2.1 Spallart Allmars (S-A)

The S-A turbulence model is a one-equation model, designed for aerospace applications. It is quite robust and effective in modelling the flow on an airfoil, with adverse pressure gradients in the boundary layer (Spalart and Allmaras, 1992; Versteeg and Malalasekera, 2007). The modified continuity equation for S-A solves the turbulent viscosity $\tilde{v}$.

$$\frac{\partial}{\partial t}\rho\tilde{v} + \frac{\partial}{\partial x_i}(\rho\tilde{v}u_i) = G_v = \frac{1}{\sigma\tilde{v}}\left[\frac{\partial}{\partial x_j}\left\{(\mu + \rho\tilde{v})\frac{\partial\tilde{v}}{\partial x_j}\right\} + C_{b2\rho}\left(\frac{\partial\tilde{v}}{\partial x_j}\right)^2\right] - Y_v + S\tilde{v} \tag{5}$$

G_v is the production of turbulent viscosity and Y_v is the destruction of turbulent viscosity.

The turbulent viscosity is calculated as:

$$\mu_t = \rho\tilde{v}f_{v1} \tag{6}$$

The f_{v1} is the viscous damping function

$$f_{v1} = \frac{\chi^3}{\chi^3 + c_{v1}^3} \tag{7}$$

It has been reported that this model is effective for low Reynolds number cases, provided that the mesh resolution is super fine with a wall $Y^+ \leq 1$ (2015b; 2015c).

2.2.2 Standard k-ε Model

The standard k-ε model (Launder and Spalding, 1972) is based on modelling the transport equations for the turbulence kinetic energy (k) and its dissipation rate (ε). It is a two-equation turbulence model that allows the determination of both, a turbulent length and time scale by solving two separate transport equations. The model transport equation for k is derived from the exact equation, while the model transport equation for ε was obtained using physical reasoning and bears little resemblance to its mathematically exact counterpart.

In the derivation of the k-ε model, the assumption is that the flow is fully turbulent, and the effects of molecular viscosity are negligible. The standard k-ε model is therefore valid only for fully turbulent flows.

The turbulence kinetic energy, k, and its rate of dissipation, ε, are obtained from the following transport equations:

$$\frac{\partial}{\partial t}(\rho k) + \frac{\partial}{\partial x_i}(\rho k u_i) = \frac{\partial}{\partial x_j}\left[\left(\mu + \frac{\mu_t}{\sigma_k}\right)\frac{\partial k}{\partial x_j}\right] + G_k + G_b - \rho\varepsilon - Y_M + S_k \tag{8}$$

and

$$\frac{\partial}{\partial t}(\rho\varepsilon) + \frac{\partial}{\partial x_i}(\rho\varepsilon u_i) = \frac{\partial}{\partial x_j}\left[\left(\mu + \frac{\mu_t}{\sigma_\epsilon}\right)\frac{\partial\varepsilon}{\partial x_j}\right] + C_{1\varepsilon}\frac{\varepsilon}{k}(G_k + C_{3\varepsilon}G_b) - C_{2\epsilon}\rho\frac{\varepsilon^2}{k} + S_\varepsilon \tag{9}$$

Where G_k represents the generation of turbulence kinetic energy due to the mean velocity gradients, G_b is the generation of turbulence kinetic energy due to buoyancy, Y_M represents the contribution of the fluctuating dilatation in compressible turbulence to the overall dissipation rate, $C_{1\varepsilon}$, $C_{2\varepsilon}$, and $C_{3\varepsilon}$ are constants. σ_k and σ_ε are the turbulent Prandtl numbers for k and ε, respectively. S_k and S_ε are user-defined source terms.

The turbulent viscosity, μ_t, is computed by combining k and ε as follows:

$$\mu_t = \rho C_\mu \frac{k^2}{\epsilon} \tag{10}$$

140   Where C_μ is a constant.

The default values of the model constants are (Launder and Spalding, 1972):

$C_{1\varepsilon}$=1.44, $C_{2\varepsilon}$=1.92, C_μ=0.09, σ_k=1.0 and σ_ε=1.3

2.2.3 The RNG k-ε model

The RNG k-ε model was derived using a statistical technique called renormalization group (RNG) theory. It is similar in form

145   to the standard k-ε model, but includes the following refinements:

- The RNG model has an additional term in its equation that improves the accuracy for rapidly strained flows.
- The effect of swirl on turbulence is included in the RNG model, enhancing accuracy for swirling flows.
- The RNG theory provides an analytical formula for turbulent Prandtl numbers, while the standard k-ε model uses user-specified, constant values.

150   - While the standard k-ε model is a high-Reynolds number model, the RNG theory provides an analytically-derived differential formula for effective viscosity that accounts for low-Reynolds number effects. Effective use of this feature does, however, depend on an appropriate treatment of the near-wall region.

These features make the RNG k-ε model more accurate and reliable for a wider class of flows than the standard k-ε model.

The RNG-based k-ε turbulence model is derived from the instantaneous Navier-Stokes equations, using a mathematical

155   technique known as RNG method. A more comprehensive description of RNG theory and its application to turbulence can be found in (Orszag et al., 1993).

2.2.4 Standard k-ω Model

The standard k-ω model is an empirical model based on model transport equations for the turbulence kinetic energy (k) and the specific dissipation rate (ω), which can also be thought of as the ratio of ω to k (Wilcox, 1998). One of the weak points of

160   the Wilcox model is the sensitivity of the solutions to values for k and ω outside the shear layer (freestream sensitivity). As the k-ω model has been modified over the years, production terms have been added to both the k and ω equations, which have improved the accuracy of the model for predicting free shear flows. The new formulation implemented in ANSYS Fluent has reduced this dependency, it can still have a significant effect on the solution, especially for free shear flows (Menter, 2009).

The turbulence kinetic energy, k, and the specific dissipation rate, ω, are obtained from the following transport equations:

165
$$\frac{\partial}{\partial t}(\rho k) + \frac{\partial}{\partial x_i}(\rho k u_i) = \frac{\partial}{\partial x_j}\left[\Gamma_k \frac{\partial k}{\partial x_j}\right] + G_k - Y_k + S_k \tag{11}$$

and

$$\frac{\partial}{\partial t}(\rho \omega) + \frac{\partial}{\partial x_i}(\rho \omega u_i) = \frac{\partial}{\partial x_j}\left[\Gamma_\omega \frac{\partial \omega}{\partial x_j}\right] + C_\omega - Y_\omega + S_\omega \tag{12}$$

Where G_k represents the generation of turbulence kinetic energy due to mean velocity gradients. G_ω represents the generation of ω. Γ_k and Γ_ω represent the effective diffusivity of k and ω, respectively. Y_k and Y_ω represent the dissipation of k and ω due

170   to turbulence. All of the above terms are calculated as described below. S_k and S_ω are user-defined source terms.

2.2.5 Shear-Stress Transport (SST) k-ω model

The shear-stress transport (SST) k-ω model was developed by Menter (Menter, 1994). It is a combination of the Wilcox K-ω and the standard K-ε model. It is so named because the definition of the turbulent viscosity is modified to account for the transport of the principal turbulent shear stress. The standard k-ε is transformed to k-ω by substituting $\varepsilon = k\omega$ (Versteeg and

175   Malalasekera, 2007). It has features that give the SST k-ω model an advantage in terms of performance over both the standard k-ω model and the standard k-ε model. Other modifications include the addition of a cross-diffusion term in the ω equation

and a blending function to ensure that the model equations behave appropriately in both the near-wall and far-field zones (2015b; 2015c).

The SST k-ω model has a similar form to the standard k-ω model. The turbulence kinetic energy, k, and the specific dissipation rate, ω, are obtained from the following transport equations:

$$\frac{\partial}{\partial t}(\rho k) + \frac{\partial}{\partial x_i}(\rho k u_i) = \frac{\partial}{\partial x_j}(\Gamma_k \frac{\partial k}{\partial x_j}) + \widetilde{G}_k - Y_k + S_k \tag{13}$$

and

$$\frac{\partial}{\partial t}(\rho \omega) + \frac{\partial}{\partial x_i}(\rho \omega u_i) = \frac{\partial}{\partial x_j}(\Gamma_\omega \frac{\partial \omega}{\partial x_j}) + G_\omega - Y_\omega + D_\omega + S_\omega \tag{14}$$

where

G_k represents the generation of turbulence kinetic energy due to mean velocity gradients. G_ω represents the generation of ω. Γ_k and Γ_ω represent the effective diffusivity of k and ω, respectively. Y_k and Y_ω represent the dissipation of k and ω due to turbulence. D_ω represents the cross-diffusion term. S_k and S_ω are user-defined source terms. Calculations for all previous terms have been fully described in (2015b; 2015c).

2.2.6 The Reynolds Stress Model (RSM)

The Reynolds stress model (RSM) (Launder et al., 1975; Launder, 1989; Gibson and Launder, 1978) is the most elaborate type of RANS turbulence model that ANSYS Fluent provides. Abandoning the isotropic eddy-viscosity hypothesis, the RSM closes the RANS equations by solving transport equations for the Reynolds stresses, together with an equation for the dissipation rate. This means that five additional transport equations are required in 2D flows, in comparison to seven additional transport equations solved in 3D.

Since the RSM accounts for the effects of streamline curvature, swirl, rotation, and rapid changes in strain rate in a more rigorous manner than one-equation and two-equation models, it has greater potential to give accurate predictions for complex flows. However, the fidelity of RSM predictions is still limited by the closure assumptions employed to model various terms in the exact transport equations for the Reynolds stresses. The modeling of the pressure-strain and dissipation-rate terms is particularly challenging, and often considered to be responsible for compromising the accuracy of RSM predictions.

2.3 Numerical Simulation Setup

Generating the right computational domain for a fluid dynamic problem is an important task of the modeling process. It is necessary to take into account different requirements (Blazek, 2015). The domain should not be too small to correctly reproduce the flow around the airfoil or too large to adequately increase cells number of the grid, and hence computation time (Lanzafame et al.). It is preferable to perform independency study to select the suitable domain/grid for your case study. It should to be taken into account the requirements of the meshing in terms of quality and first cell positioning near the airfoil.

Mesh properties include mesh types, computational domain sizes, and node distributions are important in CFD simulation. Suli Lu et al. (Lu et al., 2021) suggest recommended Reynolds numbers, domain sizes, and near- and far-field node distributions for mesh types with distinct topology structures, i.e., C-mesh, O-mesh, H-mesh, and Hybrid-mesh.

The Ansys R17 package is used to simulate the air flow characteristics over DTU-LN221 airfoil. The 2-D Design Modeler (DM) is used to draw the airfoil profile by using the coordinates of 300 points to guarantee the smoothness and accuracy of the airfoil profile. The computational domain is composed of an upstream C-shape, half of circle, in which the airfoil is included. The airfoil end is located at the center of the semicircle. The C-shape is preferable over the other structures because it gives better convergence of flow over the airfoil. It helps to control the wall plus function of the mesh to give good result. In addition, it improves the skew and orthogonality of the mesh. The diameter of the semicircle of the C-shape is 10 times the

215 chord of the airfoil (G. et al., 2004; Wang et al., 2014; Chaudhary and Nayak, 2015). The downstream domain is square with side lengths equaling the circle diameter as shown in Fig. 3. C-type structured grid is applied in the airfoil domain to consider the boundary layer's effect on the aerodynamic performance of airfoils. Also considering the requirements of turbulence model for the grid, the boundary layer mesh is denser around the airfoil.

The mesh is constructed by Ansys Mesh. 2-D curvature, fine, high smoothing mesh with a growth rate of 1.05 is constructed.
220 Different edges and face sizing are chosen to build up different meshes with different number of elements to check the independency of the results.

In general, the finer the mesh, the more accuracy of the solution. A mesh independency study is conducted to verify that the solution obtained numerically is not dependent on the mesh density. Six different grids were created. A mesh series of approximately 108700, 63000, 51000, 36000, 24000 and 16000 cells have been designed, respectively. The only change is in
225 the mesh sizing. The other mesh setting was not changed. Both lift and drag dimensionless coefficients were calculated at 5° AOA for the six grids using RSM. The results are shown in Fig. 2 where the grid with 24000 cells generated the same results as the higher number of cell grids. The exact total number of model grid was 23897 elements. It is apparent from the figure below that the distribution of the grid was much denser in airfoil's front edge, back edge and airfoils surface. The mesh of the computational domain was shown in Fig 3.a. Airfoil and nearby wall grid were shown in Fig 3.b.

230

Figure 2: Mesh indecency for RSM

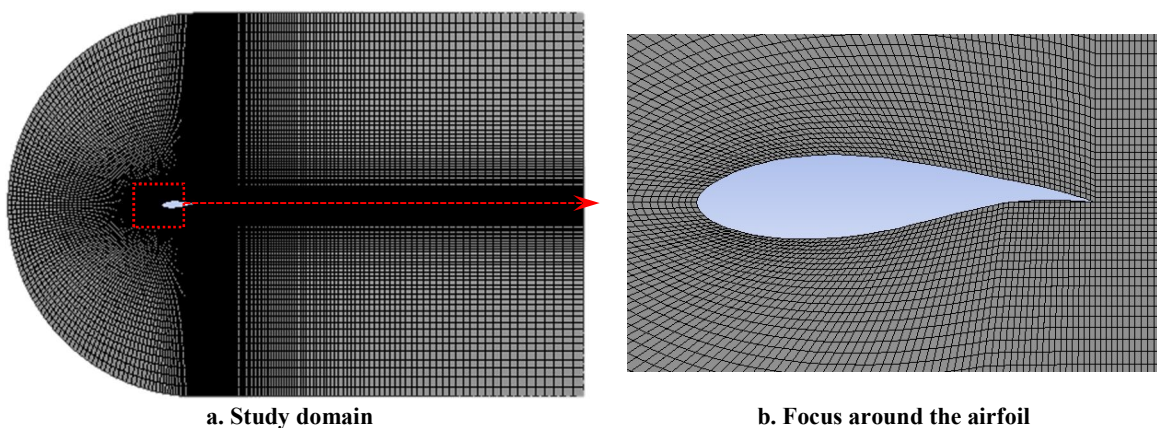| a. Study domain | b. Focus around the airfoil |
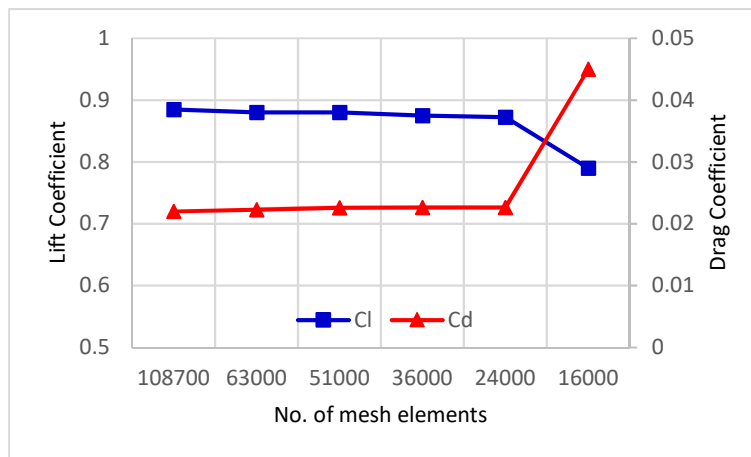
Figure 3: The integral mesh grid

To validate the simulation of the DTU-LN221 airfoil, six turbulence models are applied to numerically simulate under the
235 same conditions of Re number, temperature, and turbulence intensity. The air velocity is 37.5 m/s which generates a turbulence with Re of 1.8×10^6. 2D, double precession, serial processing options are chosen. Density based, SIMPLE algorithm is used in

processing coupling problems of speed and pressure in FLUENT solver. The second-order upwind scheme is used to discrete the fluxes in the governing equations. It also provides the best balance between solution accuracy and robustness. The Energy Equation is functioning and air is considered as an ideal gas. The initial and boundary conditions are shown in Table 2.

240

Table 2 : Initial and Boundary Conditions

Boundary Conditions	Type	Variables	notes
inlet	Velocity Inlet	V= 37.5 m/s T= 293 K P_g= 0 kPa (atmospheric conditions) T.I. = 0.0011 Turbulent viscosity ratio =10	x and y components of velocity are varied according to AOA
Outlet	Pressure Outlet	T= 293 K P_g= 0 kPa (atmospheric conditions) T.I. = 0.0011 Turbulent viscosity ratio =10	
Airfoil surface	Wall	Stationary wall Non slip Zero roughness	
Viscous Model	Alternate: S-A, k-ε, RNG k-ε, k-ω, SST k-ω and RSM.		
Other Conditions	Air density: ideal gas Airfoil Chord: 0.6 m Reference Length = 1.5 m (Used in defining the reference values) AOA : varied from -10º to 20º		

3 Results and Discussions

3.2 Lift and Drag Coefficients

The flow around the blade airfoil of wind turbines generates a force with two main components:

245 Lift force: it the component of force that acts perpendicular to the oncoming airflow. It is a result of the unequal pressure on the upper and lower airfoil surfaces. It is given by:

$$F_L = C_L \left(\tfrac{1}{2}\rho A V^2 \right) \tag{15}$$

Where C_L is the lift force coefficient ρ is the density of air, A is the projected airfoil area (Chord x span), V is the velocity of the undistributed air flow and ($\tfrac{1}{2}\rho V^2$) is the dynamic pressure.

250 Drag Force: it the component of force that acts in the parallel direction to the oncoming airflow. It is a result of both viscous friction forces at the surface of the airfoil and the unequal pressure on the upper and lower airfoil surfaces. It is given by:

$$F_D = C_D \left(\tfrac{1}{2}\rho A V^2 \right) \tag{16}$$

Where C_D is the drag force coefficient and ($\tfrac{1}{2}\rho V^2$) is the dynamic pressure.

Six viscous models are used to simulate the flow over DTU-LN221 airfoil. These models are S-A, k-ε, RNG k-ε, k-ω, SST k-

255 ω and RSM. The lift and drag coefficients are monitored for each simulation. The results are compared with the experimental findings in (Roha, 2012; Yang et al., 2020). The experimental measured data of the airfoil were corrected by the reference (Allen and Vlncenti, 1944). The experimental values of the lift and drag coefficients of the selected airfoil are compared with the simulated lift and drag coefficients of the six turbulence models respectively.

Fig. 4 shows the comparison of the lift coefficients simulated by six turbulent models and the theoretical lift coefficient. In

260 general, lift force increases with AOA and reaches to the maximum value at an AOA of (10º~12º) in this type of airfoil. After this point, the lift coefficient decreases with further increase of AOA due to entering the airflow in turbulent region, which separates the boundary layers from the airfoil. Therefore, the drag force rapidly goes up and the lift force goes down in this region.

8

In order to verify the simulation results of lift coefficients of six turbulent models, the flow fields given by six turbulent models are also given subsequently as Fig. 6. According to Fig. 4, the simulated lift coefficients of the experimental value and the six different turbulence models are very close during the AOA of -5°: 5° range and more consistent with the experimental values. Lift coefficients increase nearly linearly with the increasing attack angle when the AOA is smaller than 10°. The lift coefficients results of the six turbulence models show significant differences when the AOA is bigger than 10°.

One possible reason for the deviation between the experimental data and the simulation results may be due to the roughness of the airfoil surface that can affect the experimental results. The pressure of the air fan in the wind tunnel may also affect the simulation results as it was purposely excluded. In addition, the effect of flow separation may affect the drag force considerably. Airfoil flow separates when airfoil is at a high AOA, which is caused by the viscosity of fluid.

From Fig. 4, it can be noticed that the results can be divided into four regions:

i. AOA < -5° region: in this region, the simulation findings for all of the six models approximately gave the same value of lift coefficients. All were greater than the lift coefficient that was calculated by experiments data. The nearest values to the experiments were given by SST k-ω and RSM.

ii. -5° < AOA < 5° region: good results compared with the experimental findings are produced. RSM shows the best approximation while k-ε and S-A models performed the worst.

iii. 5° < AOA < 10° region: the simulation findings start to deviate gradually from the experimental findings. RSM still shows the best approximation while k-ε and S-A models are still the worst. At an AOA of 10° the lift coefficient resulted from RSM simulation was less than that resulted from experiments by about 13.5%. Whereas for S-A model, this percentage reached 22%.

iv. AOA > 10° region: there is a clear diversity of the performance results where the k-ω and RSM provided good results with respect to the experimental data while S-A model still performed the worst.

Fig. 5 shows the comparison of drag coefficient using different viscous models. It is shown that the drag coefficients was small up to AOA<10°. Then the drag increased rapidly with the increase of AOA. The RSM model gave the best results for drag coefficient while the worst results were delivered by k-ε model.
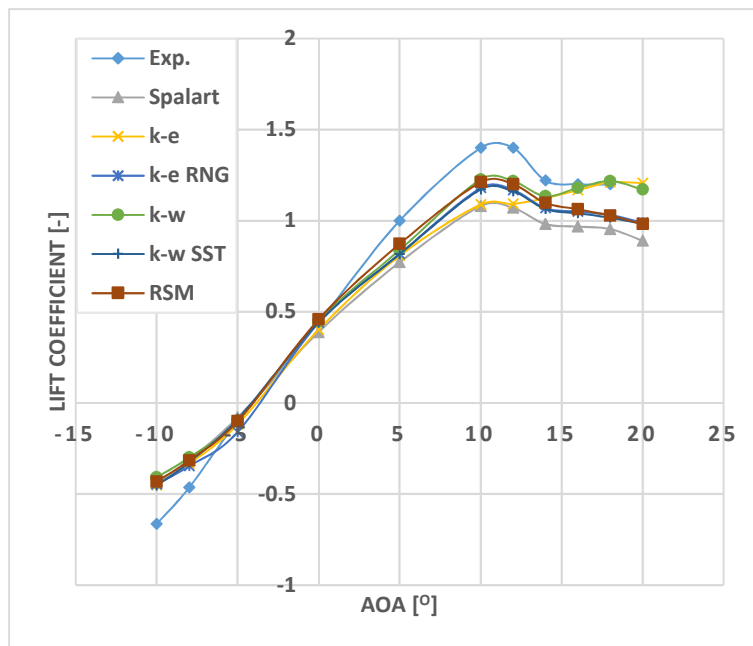

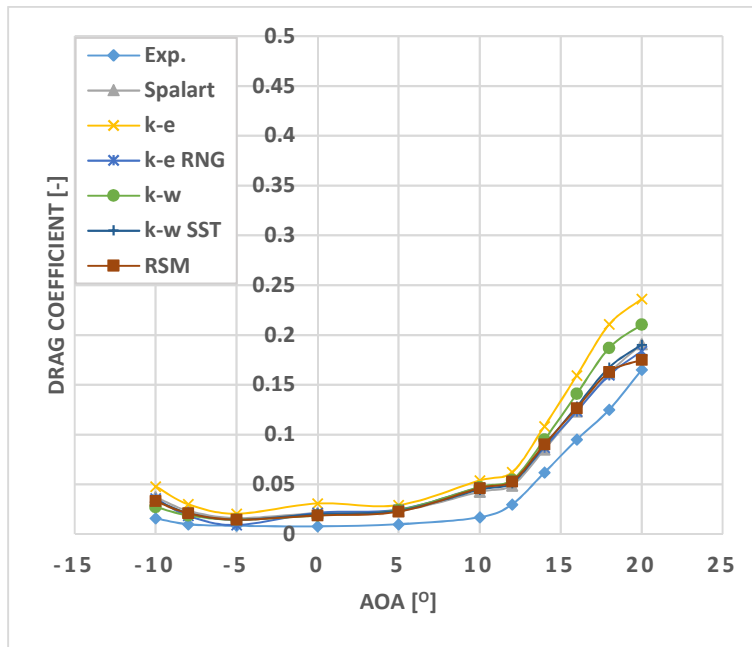**Figure 4: The comparison of lift coefficient using different models**

Figure 5: The comparison of drag coefficient using different models

3.3 Effect of Angle of Attack (AOA) on the Flow Field

RSM is applied to simulate the fluid field at different AOA. Four AOAs (-5º, 0º, 5º, and 10º) are chosen to show the flow field represented by pressure and velocity distributions.

Fig. 6 shows the flow fields of wind turbine blade airfoil with different AOA. As the AOA increases, the pressure in the lower side of the airfoil increases while the velocity decreases. On the other side, the upper side, the pressure difference to ambient is positive with an AOA of -5º whereas negative pressure contours emerged in zero and positive AOA. With the decrease of the pressure on the upper side of the airfoil, the velocity increases. The design of such airfoil benefits from having extra lift force from the tail of the airfoil as well as the front head.

The flow field of the trailing edge of the wind turbine blade airfoil shows that the flow is applicable to attached flow for the four conditions of AOA, and there are no turbulence or flow separations at all. That is why the simulation results of aerodynamic performance of blade airfoil using this turbulent model is similar and coincides with the experimental values considerably.
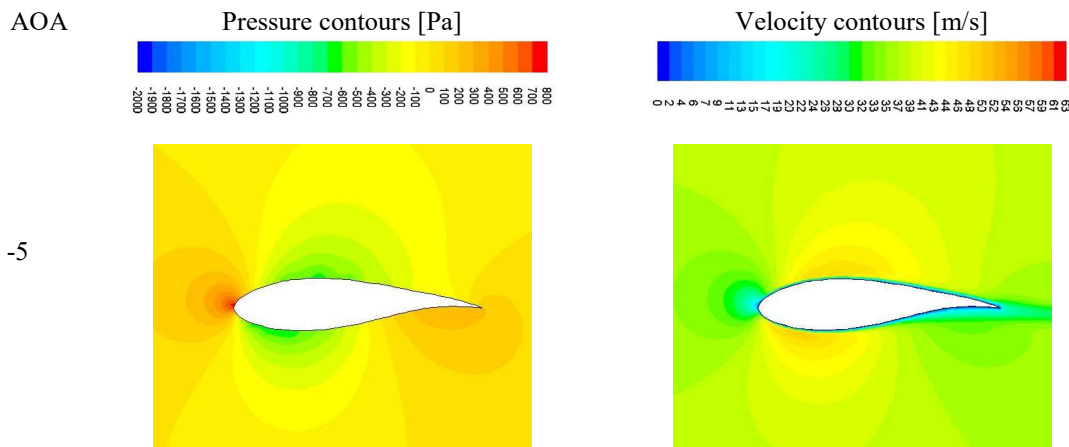
Figure 6: The flow fields of wind turbine blade airfoil with different AOA
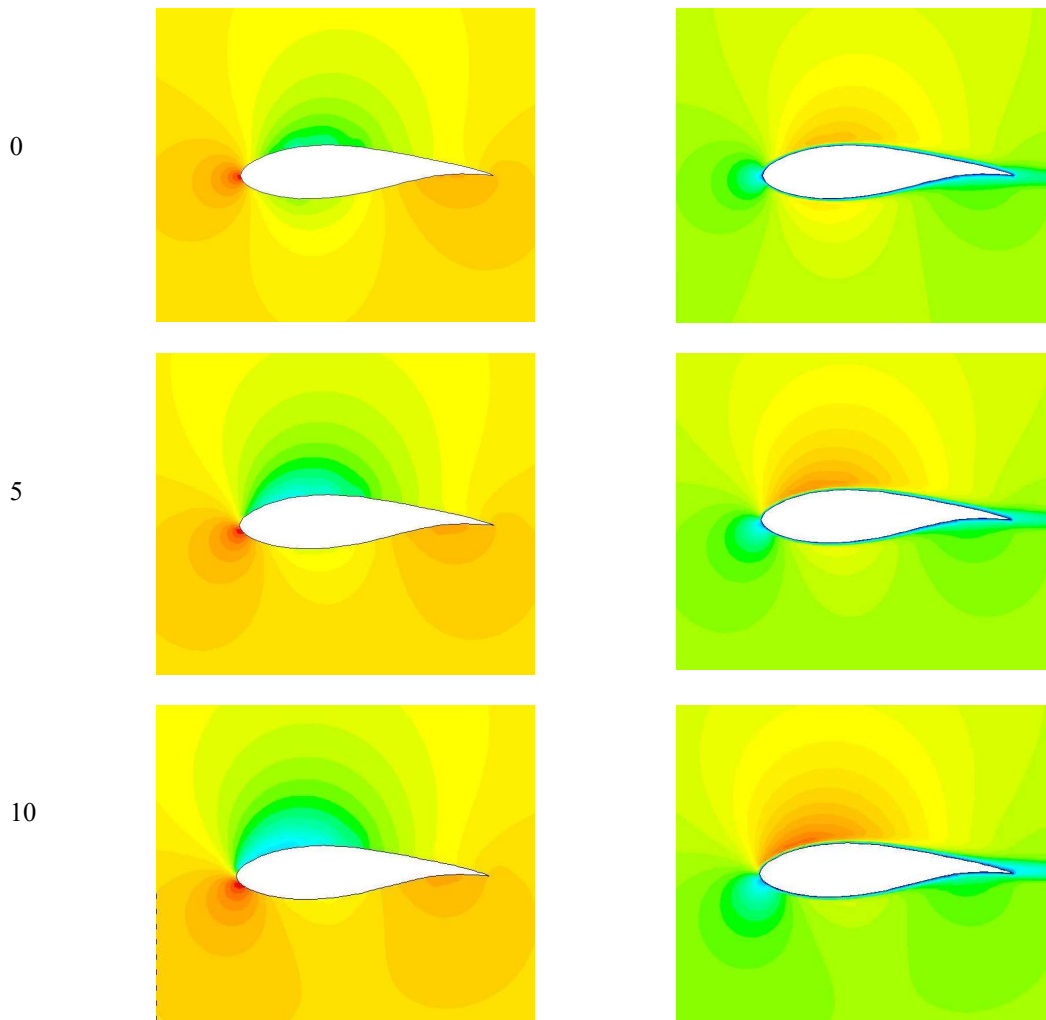
Figure 6: The flow fields of wind turbine blade airfoil with different AOA (continue)

3.4 Pressure Coefficient

The pressure coefficient C_p on the airfoil surface is defined as:

$$C_p = \frac{p_i - p_o}{\frac{1}{2}\rho U_o^2} \tag{17}$$

where p_i is the pressure at position i , p_o is the free stream static pressure at the airfoil, ρ is the air density and U_o is the free stream velocity.

The distribution of pressure coefficient of DTU-LN221 airfoil under different AOA is shown in Fig 7. RSM is applied to perform the simulation. Pressure differences between upper and lower surfaces of the airfoil increases with the AOA increasing. At the front edge of airfoil, the pressure difference is higher compared to the rear edge where the lift is produced. It can be seen in this figure that the airfoil's leading edge had a larger curvature, therefore, the flow on the airfoil surface would have an increased acceleration, and then the static pressure would lower on the airfoil's surface. With the increase of the AOA, the differences become larger at the leading edge.

There was an anti-curvature shrinking section on the airfoil rear edge pressure side, which could lower the velocity and increase the pressure as shown also in Fig. 7, consequently the pressure coefficient of rear edge pressure side had an obvious inclination.

The figure showed that the distribution of pressure on the airfoil's surface varied largely under different attack angle. When the attack angle was less than zero, the pressure coefficient of the airfoil's upper surface was positive and lower surface was negative, indicating that at this time lift force of the airfoil pointed downward. It can be seen in Fig. 7 that the larger the attack angle the greater difference of pressure coefficient between upper and lower surfaces. For DTULN221 airfoil, the difference of pressure coefficient on the airfoil's front edge was much larger, while the rear edge was much lower, indicating that the lift

11

force of the airfoil comes primarily from the front edge. For this type of airfoil, and when the attack angle is zero the pressure coefficient of the airfoil's upper and lower surface is not equal, as the DTU-LN221 airfoil is not symmetrical. Furthermore, when the attack angle was larger than zero, the pressure coefficient of airfoil's upper surface was negative and lower surface was positive, indicating that at this time the lift force of the airfoil pointed up.
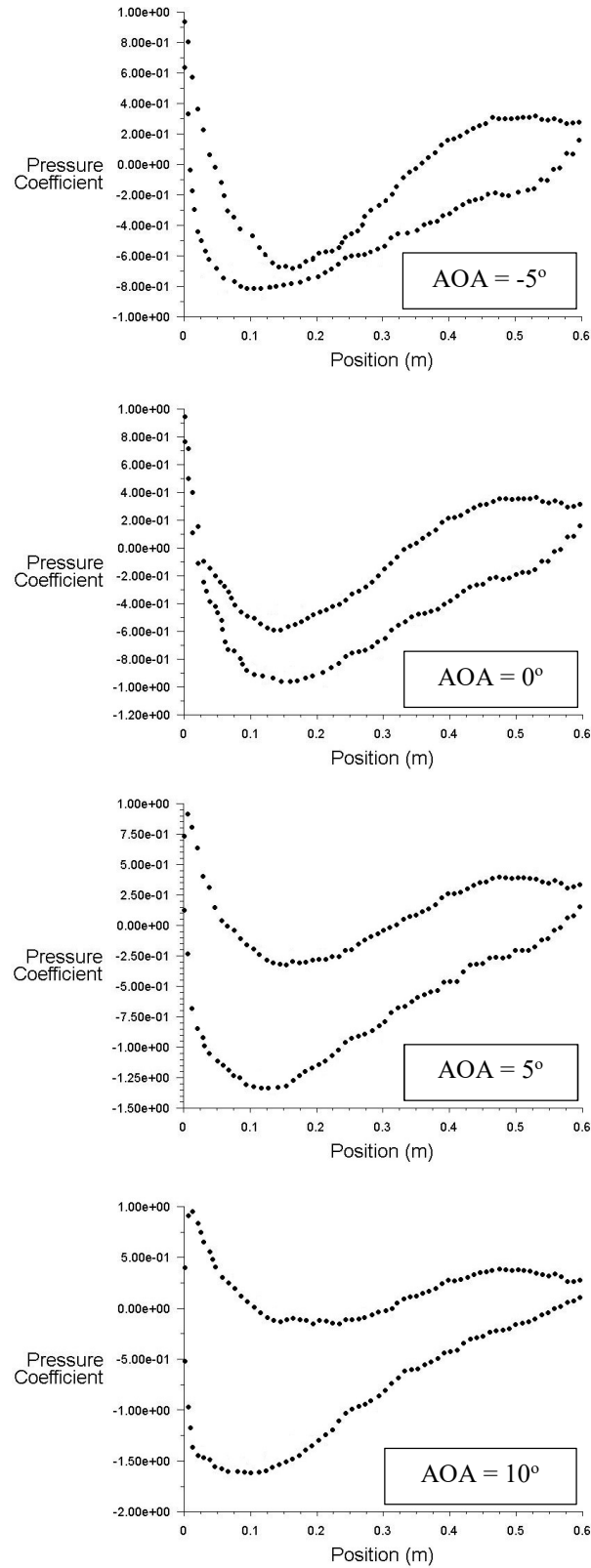
Figure 7: The surface pressure coefficients under different angle of attack

3.5 Effect of Air Temperature

RSM is used to investigate the effect of changing air temperature on the airfoil characteristics. Both lift and drag coefficients are monitored at different air temperatures. The temperature range was from 283 K to 323 K with step 10 K. Air velocity remains constant with a value of 37.5 m/s and turbulence intensity of 0.0011. Fig. 8 shows the comparison of lift coefficient under different air temperature. The lift coefficients are close to each other within a small variation. Also, there was no noticeable change in the drag coefficients with the variation of air temperature as shown in fig. 9.

The lift and drag coefficients are not the only variables that affect the behavior of the wind turbine but also lift and drag forces. The power delivered from the wind turbine depends on both lift and drag forces. Therefore, it is important to study the effect of other operating variables on lift and drag forces.

Fig. 10 shows the comparison of lift force under different air temperature. The lift force decreases with the increase of air temperature due to the decrease of air density with temperature. It is important to simulate the airfoil with a model that take the variation of the density of air with temperature. The decrease of lift force with temperature leads to a loss in power on high temperature days or in high temperature locations that may be considered in site selection for installing the wind turbine. The loss in the magnitude of the lift force is higher with the increase of AOA.

Fig. 11 shows the comparison of drag force under different air temperature. The drag force decreases with the increase of air temperature.
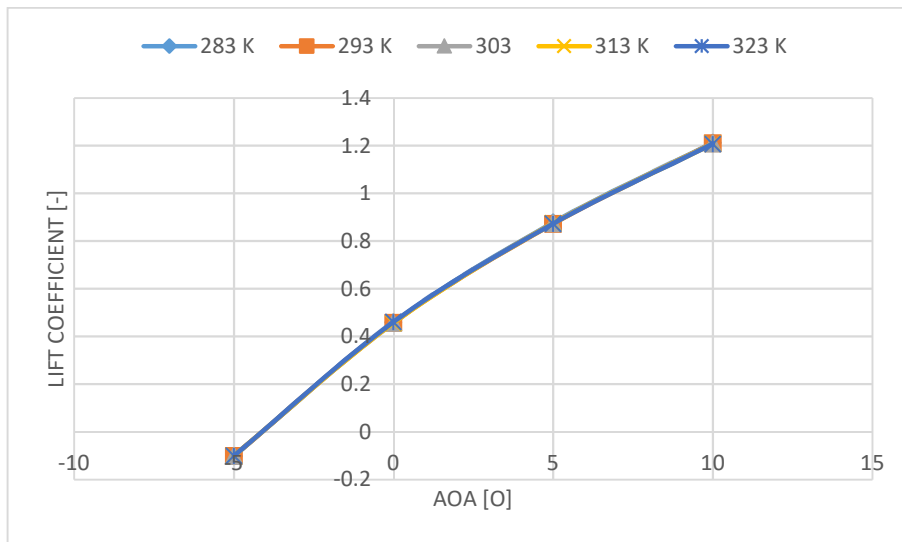

Figure 8: The comparison of lift coefficient under different air temperature
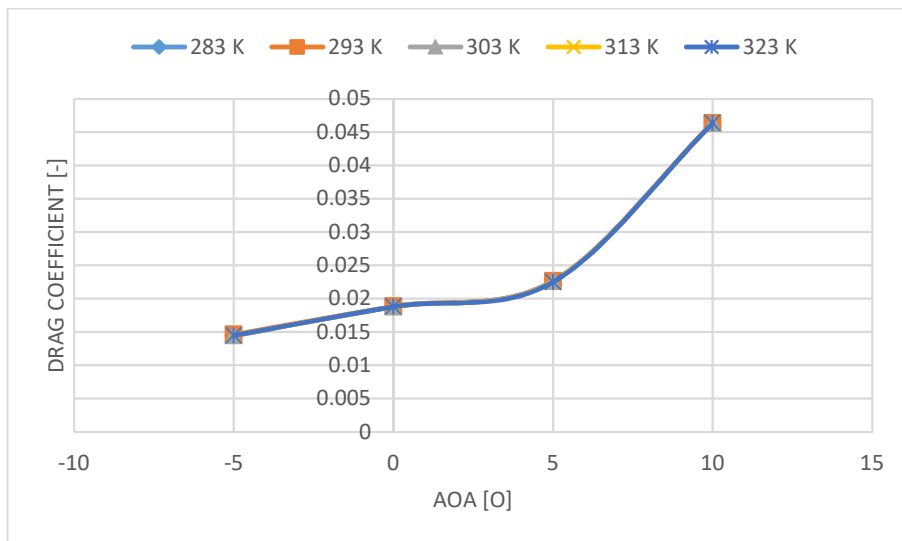

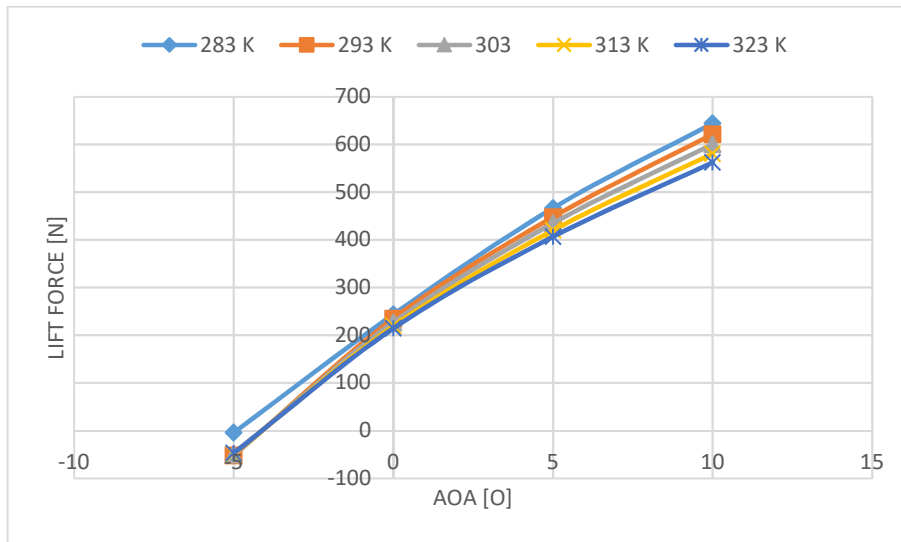**Figure 9: The comparison of drag coefficient under different air temperature**

13

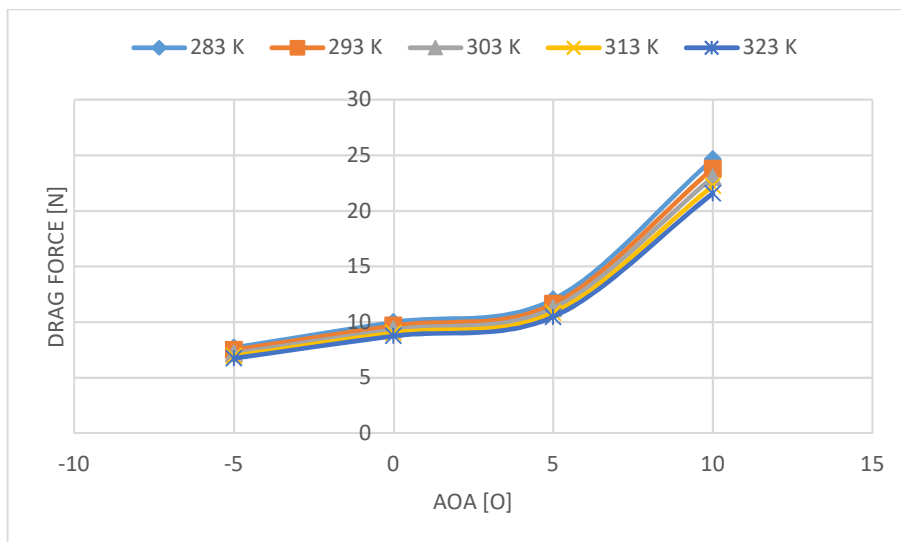**Figure 10: The comparison of lift force under different air temperature**

Figure 11: The comparison of drag force under different air temperature

3.6 Effects of Air Speed

RSM is used to investigate the effect of changing air speed on the airfoil characteristics. Both lift and drag coefficients are monitored at different air velocity. The velocities are (10, 20, 30, 37.5 and 50) m/s. Hence, the Re changes. The air temperature remains constant with a value of 293 K and the turbulence intensity is 0.0011. Fig. 12 shows the comparison of lift coefficient under different air velocity. The lift coefficient increases with the increase of air velocity. The percentage in the increase of the lift coefficients at an AOA of 10° is more significant compared with the change of lift coefficient at a lower AOA. There is a small change in the drag coefficients with the variation of air velocity as shown in fig. 13.

Fig. 14 shows the comparison of lift force under different air velocity. The lift force increases with the increase of air velocity. The rate of change at an AOA of 10° is much considerable and about three times of that at 0° angle of attack. The increase in the lift force is proportional with the square of velocity so it is preferred to operate the wind turbines at higher air velocity.

Fig. 15 shows the comparison of drag force under different air velocity. The drag force increases with the increase of air velocity.
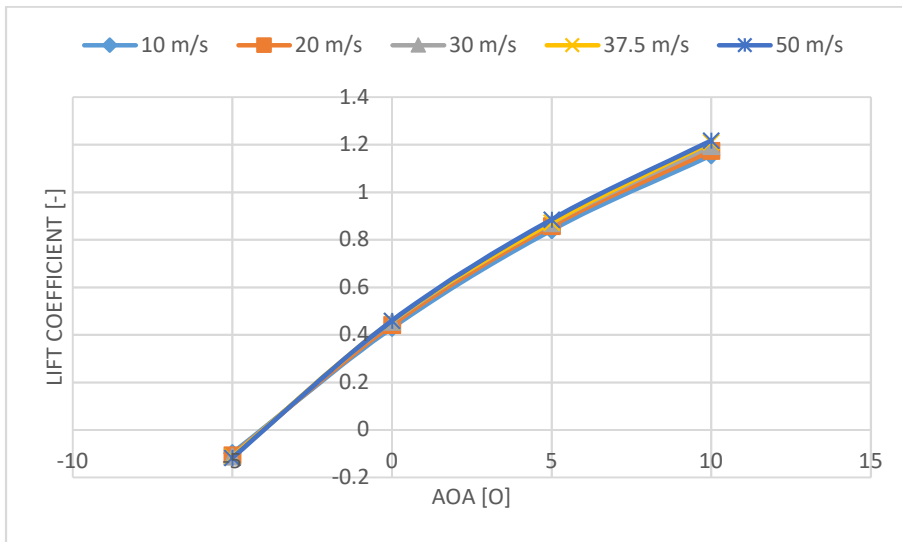
14

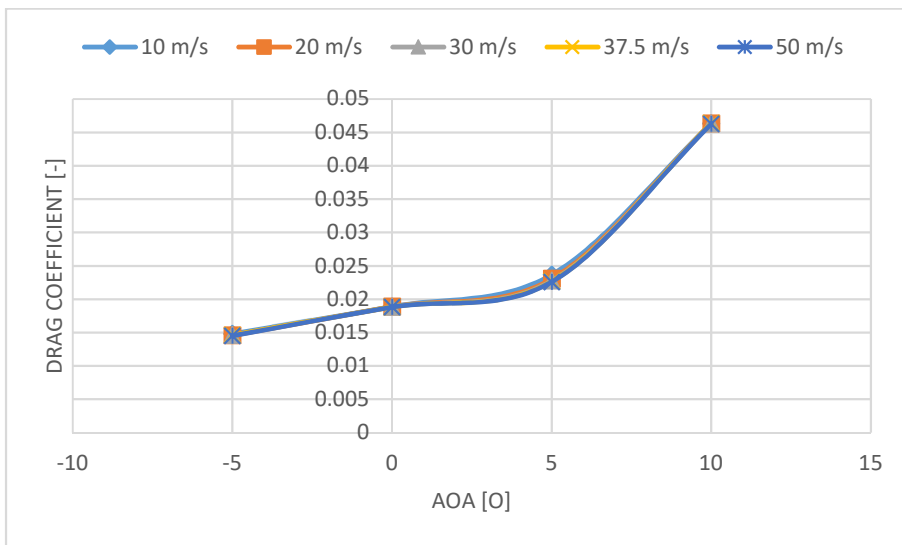**Figure 12: The comparison of lift coefficient under different air velocity**

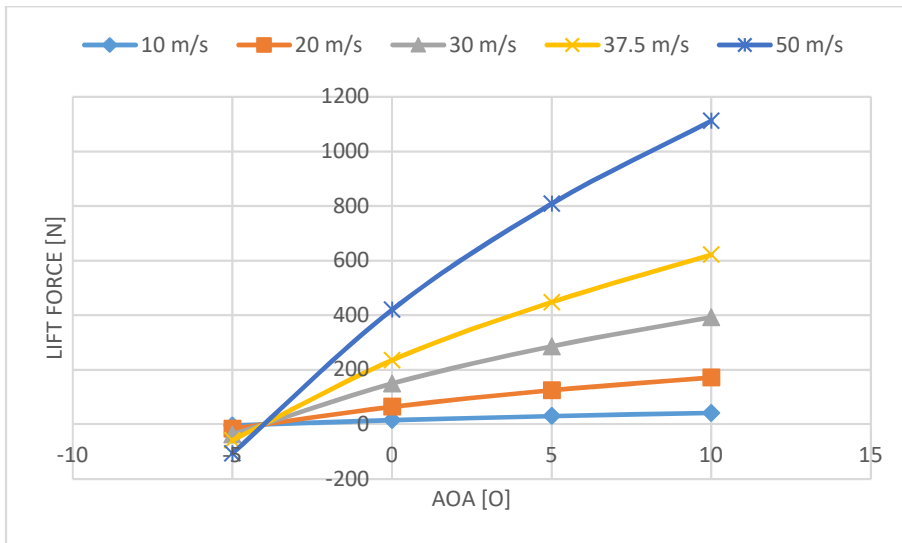**Figure 13: The comparison of drag coefficient under different air velocity**

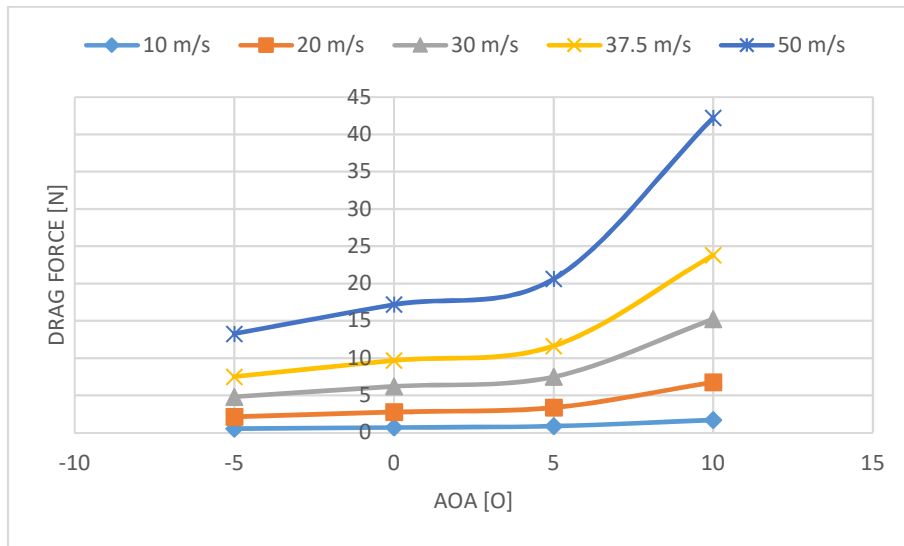**Figure 14: The comparison of lift force under different air velocity**

15

Figure 15: The comparison of drag force under different air velocity

3.7 Effect of Turbulence Intensity

The effect of changing air flow turbulence intensity on the airfoil characteristics is investigated by simulating the airfoil with RSM as a turbulence model. Both lift and drag coefficients are monitored at different turbulence intensity of 0.0011, 0.1, 1 and 2. Air velocity remains constant with a value of 37.5 m/s and temperature of 293 K. Fig. 16 shows the comparison of lift coefficient under different turbulence intensity. The lift coefficients are adjoining with a very small variation and is in direct correlation with the turbulence intensity. Also, there was no noticeable change in the drag coefficients with the variation of turbulence intensity as shown in fig. 17.

Fig. 18 shows the comparison of lift force under different turbulence intensity. The lift force does not change significantly with the change of the turbulence intensity.

Fig. 19 shows the comparison of drag force under different turbulence intensity. The drag force does not change significantly with the change of the turbulence intensity.
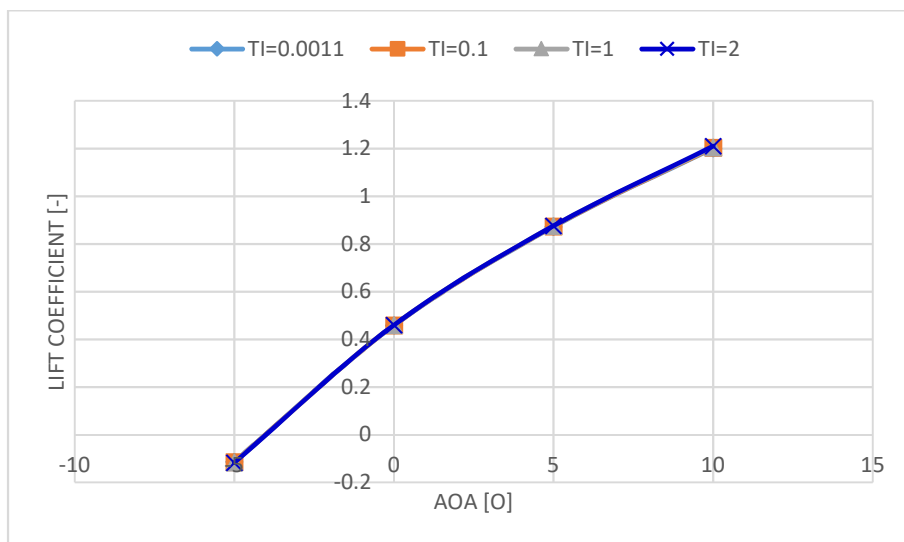

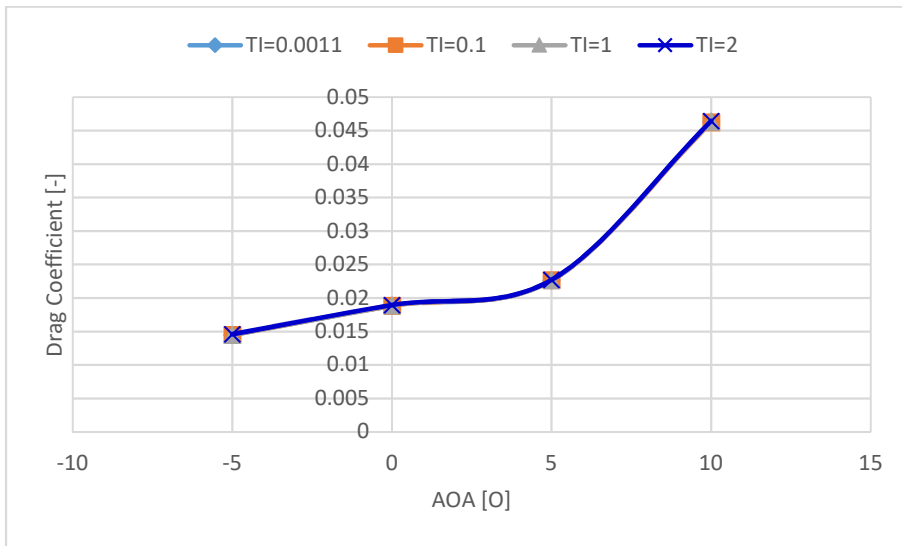**Figure 17: The comparison of lift coefficient under different air turbulence intensity**

16

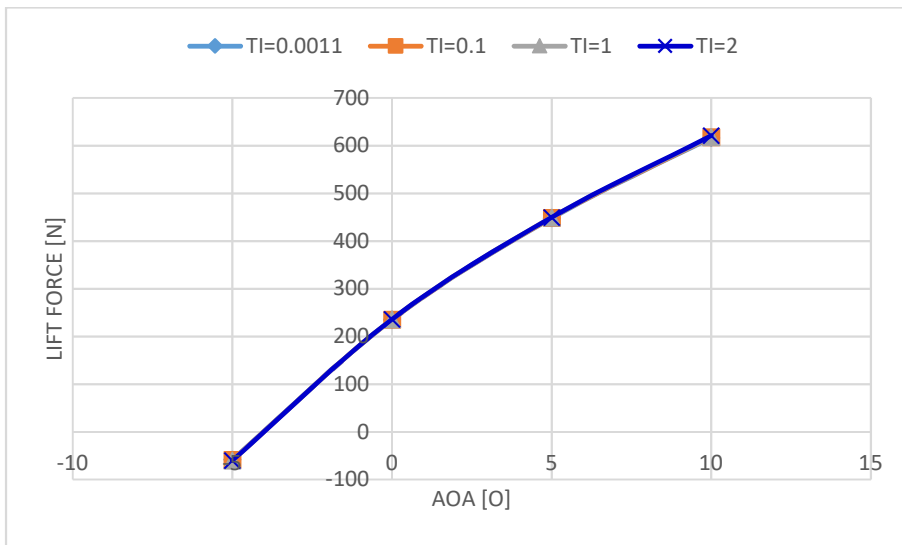**Figure 17: The comparison of drag coefficient under different air turbulence intensity**

Figure 18: The comparison of lift force under different air turbulence intensity
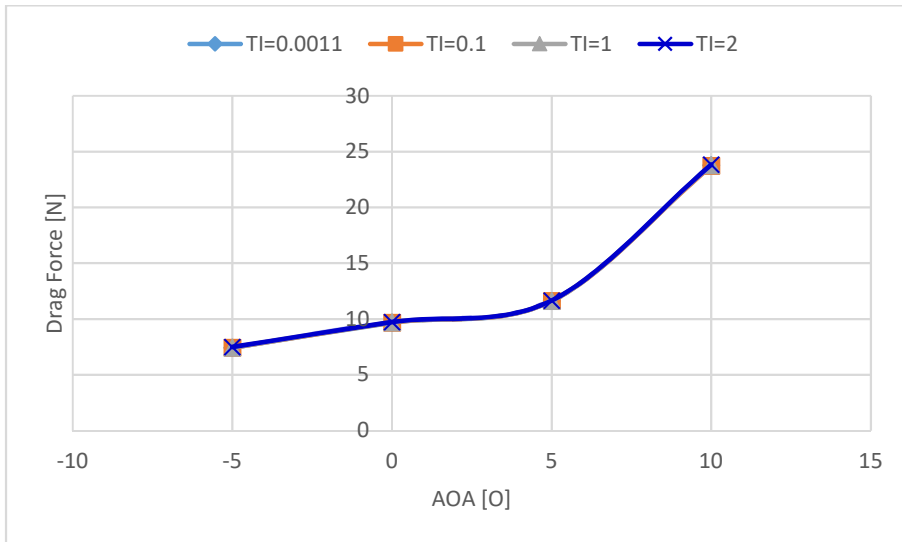

Figure 19: The comparison of drag force under different air turbulence intensity

4 Conclusion

A numerical simulation study of the aerodynamic performance of DTU-LN221 airfoil is presented. The turbulence model has a greatly definite influence on the numerical simulation results of wind turbine blade airfoil. Six turbulence models are used to simulate the flow over the airfoil. These models are S-A, k-ε, RNG k-ε, k-ω, SST k-ω and RSM. The lift and drag coefficients delivered from the simulation are compared with the wind tunnel experimental data. The range of the AOA of this simulation was between -10º to 20º. There is not a general model that can be called the best over the range of study. However, RSM presented superior results over the other turbulence models; especially in the range of AOA between -5º to 10º.

The used turbulence models succeeded to simulate the aerodynamic behavior of the air flow around the airfoil at small AOA (-5° < AOA < 5° region). The lift and drag coefficient curve are consistent with the experimental curve shape. The greater the AOA, the larger the divergence with the experimental data. The stall and separation conditions should be considered at higher AOAs.

The RSM was selected to investigate the effect of changing AOA, air temperature, velocity and turbulence intensity on the characteristics of the airfoil. CFD results produce an encouraging agreement with the experimental findings of the airfoil. The following results are confirmed with the use of RSM numerical simulation:

- By increasing the AOA (within the range of study - between -5º to 10º), the pressure in the lower side of the airfoil increases while the velocity decreases.

- The larger AOA, the greater difference of pressure coefficient between the upper and lower surface.

- Even the change in lift and drag coefficients is very small with the variation of air temperature but; there was a noticeable change in the lift and drag forces.

- The lift force decreases with the increase of air temperature.

- The lift coefficient increases with the increase of air velocity.

- The lift force increases rapidly with the increase of air velocity.

- The lift and drag forces does not change significantly with the change of the turbulence intensity.

References

Design of next generation wind turbine rotors (NextRotor), DTU Wind Energy, 2015a.

: FLUENT Ansys, Theory Guide Release 17, Ansys Inc. 2015b.

: FLUENT Ansys, User's Guide Release 17, Ansys Inc. 2015c.

Aftab, S. M. A., Rafie, A. S. M., Razak, N. A., and Ahmad, K. A.: Turbulence Model Selection for Low Reynolds Number Flows, PLoS ONE, 11, 15, 10.1371/journal.pone.0153755, 2016.

Allen, H. J. and Vlncenti, W. G.: Wall Interference in a Two-Dimensional FlowWind Tunnel, with Consideration of the effect of Compressibility, NACA Rep., 782, 155-184, 1944.

Aramendia, I., Fernandez-Gamiz, U., Zulueta, E., Saenz-Aguirre, A., and Teso-Fz-Betoño, D.: Parametric Study of a Gurney Flap Implementation in a DU91W(2)250 Airfoil, Energies, 12, 10.3390, 2019.

Blazek, J.: Computational Fluid Dynamics: Principles and Applications, Third Edition., Elsevier Ltd., https://doi.org/10.1016/C2013-0-19038-1, 2015.

Chaudhary, U. and Nayak, S.: Micro and Small-Scale HAWT Blades Airfoils Study through CFD for Low Wind Applications, 10.1109/INDICON.2015.7443703, 2015.

Cheng, J., Zhu, W. J., Fischer, A., García, N., Madsen, J., Chen, J., and Shen, W. Z.: Design and validation of the high performance and low noise CQU-DTU-LN1 airfoils, Wind Energy, 17, 1817-1833, 10.1002/we.1668, 2014.

G., S. J., L., F., V., R. R., and A., B.: Analysis of detailed aerodynamic field measurements using results from an aeroelastic code, Wind Energy, 7, 357-372, 2004.

Gibson, M. M. and Launder, B. E.: Ground Effects on Pressure Fluctuations in the Atmospheric Boundary Layer, J. Fluid Mech., 86, 491-511, 1978.

Hinze, J. O.: Turbulence, McGraw-Hill Publishing Co., New York 1975.

420 John D. Anderson, J.: Fundamentals of Aerodynamics, 6 th Ed., McGraw-Hill Education, New York, United States, 1130 pp. 2017.

Karthikeyan, N., Murugavel, K. K., Kumar, S. A., and S.Rajakumar: Review of aerodynamic developments on small horizontal axis wind turbine blade, Renewable and Sustainable Energy Reviews, 42, 801–822, 2015.

Lanzafame, R., Mauro, S., and Messina, M.: 2D CFD Modeling of H-Darrieus Wind Turbines using a Transition Turbulence

425 Model, 68th Conference of the Italian Thermal Machines Engineering Association, ATI2013, 45, 131-140, 2014.

Launder, B. E.: Second-Moment Closure: Present... and Future?, Inter. J. Heat Fluid Flow, 10, 282-300, 1989.

Launder, B. E. and Spalding, D. B.: Lectures in Mathematical Models of Turbulence, Academic Press, London, England 1972.

Launder, B. E., Reece, G. J., and Rodi, W.: Progress in the Development of a Reynolds-Stress Turbulence Closure, J. Fluid Mech., 68, 537-566, 1975.

430 Lu, S., Liu, J., and Hekkenberg, R.: Mesh Properties for RANS Simulations of Airfoil-Shaped Profiles: A Case Study of Rudder Hydrodynamics, Journal of Marine Science and Engineering, 9, 1062, 2021.

Menter, F. R.: Two-Equation Eddy-Viscosity Turbulence Models for Engineering Applications, AIAA Journal, 32, 1598-1605, 1994.

Menter, F. R.: Review of the SST Turbulence Model Experience from an Industrial Perspective, International Journal of

435 Computational Fluid Dynamics, 23, 2009.

Orszag, S. A., Yakhot, V., Flannery, W. S., Boysan, F., Choudhury, D., Maruzewski, J., and Patel, B.: Renormalization Group Modeling and Turbulence Simulations, International Conference on Near-Wall Turbulent Flows, Tempe, Arizona 1993.

ROHA: LSWT Campaign Report on DTU-C21; LM Internal Report, Jupitervej, Denmark, 2012.

Sessarego, M., Shen, W. Z., Sørensen, J. N., and Ramos García, N.: Design of Large Wind Turbines using Fluid-Structure

440 Coupling Technique., Wind Energy, DTU, DTU Wind Energy, 2016.

Spalart, P. and Allmaras, S.: A one-equation turbulence model for aerodynamic flows, Technical Report AIAA-92-0439. American Institute of Aeronautics and Astronautics, 1992.

Versteeg, H. K. and Malalasekera, W.: An introduction to computational fluid dynamics: the finite volume method, Pearson Education 2007.

445 Wang, H., Ding, J., Ma, B., and Li, S.: Aerodynamic simulation of wind turbine blade airfoil with different turbulence models, Jve International Ltd. Journal Of Vibroengineering, 16, 2474-2483, 2014.

Wilcox, D. C.: Turbulence Modeling for CFD, DCW Industries, Inc. , La Canada, California 1998.

Yang, J., Yang, H., Zhu, W., Li, N., and Yuan, Y.: Experimental Study on Aerodynamic Characteristics of a Gurney Flap on a Wind Turbine Airfoil under High Turbulent Flow Condition, Applied Sciences, 10, 2020.

450 Yaoa, J., Yuanb, W., Wanga, j., Xiec, J., Zhoub, H., Pengd, M., and Sund, Y.: Numerical simulation of aerodynamic performance for two dimensional wind turbine airfoils, International Conference on Advances in Computational Modeling and Simulation 2012.

Yu, G. H., Zhu, X. C., and Du, Z. H.: Numerical simulation of a wind turbine airfoil: dynamic stall and comparison with experiments, Proc. IMechE., 224, 657-677, 10.1243/09576509JPE942, 2010.

455